Multifractal detrending moving-average cross-correlation analysis

Zhi-Qiang Jiang (蒋志强)[1,2] and Wei-Xing Zhou (周炜星)[1,2,3,*]

[1]*School of Business, East China University of Science and Technology, Shanghai 200237, China*

[2]*Research Center for Econophysics, East China University of Science and Technology, Shanghai 200237, China*

[3]*School of Science, East China University of Science and Technology, Shanghai 200237, China*

(Received 7 May 2011; published 21 July 2011)

There are a number of situations in which several signals are simultaneously recorded in complex systems, which exhibit long-term power-law cross correlations. The multifractal detrended cross-correlation analysis (MFDCCA) approaches can be used to quantify such cross correlations, such as the MFDCCA based on the detrended fluctuation analysis (MFXDFA) method. We develop in this work a class of MFDCCA algorithms based on the detrending moving-average analysis, called MFXDMA. The performances of the proposed MFXDMA algorithms are compared with the MFXDFA method by extensive numerical experiments on pairs of time series generated from bivariate fractional Brownian motions, two-component autoregressive fractionally integrated moving-average processes, and binomial measures, which have theoretical expressions of the multifractal nature. In all cases, the scaling exponents h_{xy} extracted from the MFXDMA and MFXDFA algorithms are very close to the theoretical values. For bivariate fractional Brownian motions, the scaling exponent of the cross correlation is independent of the cross-correlation coefficient between two time series, and the MFXDFA and centered MFXDMA algorithms have comparative performances, which outperform the forward and backward MFXDMA algorithms. For two-component autoregressive fractionally integrated moving-average processes, we also find that the MFXDFA and centered MFXDMA algorithms have comparative performances, while the forward and backward MFXDMA algorithms perform slightly worse. For binomial measures, the forward MFXDMA algorithm exhibits the best performance, the centered MFXDMA algorithms performs worst, and the backward MFXDMA algorithm outperforms the MFXDFA algorithm when the moment order $q < 0$ and underperforms when $q > 0$. We apply these algorithms to the return time series of two stock market indexes and to their volatilities. For the returns, the centered MFXDMA algorithm gives the best estimates of $h_{xy}(q)$ since its $h_{xy}(2)$ is closest to 0.5, as expected, and the MFXDFA algorithm has the second best performance. For the volatilities, the forward and backward MFXDMA algorithms give similar results, while the centered MFXDMA and the MFXDFA algorithms fail to extract rational multifractal nature.

DOI: 10.1103/PhysRevE.84.016106 PACS number(s): 89.75.Da, 05.45.Tp, 05.45.Df, 05.40.−a

I. INTRODUCTION

Natural and socioeconomic systems are usually complex systems from which macroscopic statistical laws emerge. These macroscopic laws are the outcomes of self-organization and interactions among constituents, which cannot be explained by the sum of the microscopic behaviors of individuals. Statistical laws can be extracted from time series, which is the most usual recorded form of observable quantities in real world. The fractal and multifractal nature of time series has been extensively studied for different systems [1].

For a nonstationary time series, the detrended fluctuation analysis (DFA) can be adopted to explore its long-range autocorrelations [2–6] and multifractal features [7–9]. Alternatively, the detrending moving-average (DMA) method can also be used for fractal analysis [10–14] or multifractal analysis [15,16]. Numerical experiments on monofractal time series unveil that the performance of the DMA method is comparable to the DFA method with slightly different priorities under different situations [17–19]. However, for multifractal time series, the multifractal detrending moving average (MFDMA) performs better than the multifractal detrended fluctuation analysis (MFDFA) [15]. In addition, we note that both the DFA and DMA algorithms can be extended from one dimension to higher dimensions for fractal and multifractal analysis [15,20–22].

A complex system usually contains several observable variables that exhibit long-range dependence or multifractal nature. In turbulent flows, the velocity, temperature, and concentration fields are embedded in the same space as joint multifractal measures [23–27], in which the scaling behavior of the joint moments of two joint multifractal measures μ_1 and μ_2 is investigated:

$$J(s) = \langle [\mu_1(s)]^p [\mu_2(s)]^q \rangle, \tag{1}$$

where s is the box size. This framework has also been applied to study the joint multifractal nature between topographic indices and crop yield in agronomy [28,29], trading volume and volatility in stock markets [30], nitrogen dioxide and ground-level ozone [31], heart rate variability and brain activity of healthy humans [32], and wind patterns and land surface air temperature [33].

For two stationary time series $\{x(i)\}$ and $\{y(i)\}$ of the same length, the time-lagged cross correlation or covariance provides another example [34–37],

$$C(s) = \langle x(t)y(t+s) \rangle. \tag{2}$$

*wxzhou@ecust.edu.cn

For two nonstationary time series $\{X(i)\}$ and $\{Y(i)\}$ of the same length, one can study the following cross-correlation function between two detrended series [38]:

$$C_{xy}(s) = \langle [X(t) - \widetilde{X}(t)][Y(t+s) - \widetilde{Y}(t+s)] \rangle, \quad (3)$$

where $\widetilde{X}(t)$ and $\widetilde{Y}(t)$ are certain trend functions of $X(t)$ and $Y(t)$, respectively. The detrended cross-correlation analysis (DCCA) was introduced to investigate the long-range power-law cross correlations between two nonstationary time series [39–41]:

$$F_{xy}(s) = \langle [X(t) - \widetilde{X}(t)][Y(t) - \widetilde{Y}(t)] \rangle, \quad (4)$$

where $\widetilde{X}(t)$ and $\widetilde{Y}(t)$ are certain trend functions of $X(t)$ and $Y(t)$ specific to moving windows of size s, respectively. The DFA method is a special case of this DCCA method when $X(t) = Y(t)$. The DCCA method studies the temporal (not the cross-sectional) properties of two nonstationary time series, which is similar to the instant cross correlations [42,43]. The significance of the cross correlation can be assessed by statistical tests [44,45]. Podobnik and Stanley pointed out that, when $F_{xy}(s)$ versus s fluctuates around zero, there are no power-law cross correlations with a unique exponent: either no cross correlations or only short-range cross correlations exist between $X(t)$ and $Y(t)$ [40]. The DCCA method has been applied to study volume change and price change of the Standard and Poor's (S&P) 500 Index [46], volatilities of the Brazilian agrarian commodities and stocks [47], traffic flows [48], and self-affine time series of taxi accidents [49]. Alternatively, the temporal cross-correlation property can also be investigated using the cross-spectral density function or the coherence function based on wavelet transform [50,51].

More generally, the multifractal detrended cross-correlation analysis was introduced to investigate the multifractal nature in the long-range power-law cross correlations between two nonstationary time series [52], which recovers the MFDFA method when $X(t) = Y(t)$. We call this method the MFXDFA for reasons that will be clear in Sec. II. Note that the MFXDFA method is relevant to the multifractal height cross-correlation analysis with differences [53]. The MFXDFA method has been applied to temporal and spatial seismic data [54], sunspot numbers and river flow fluctuations [55], stock index prices [56,57], price-volume relationships in agricultural commodity futures markets [58], prices of the Chinese and US agricultural futures [59], spot and futures markets of West Texas Intermediate (WTI) crude oil [60], and traffic signals [61].

In this work, we introduce a variant of the MFXDFA algorithm, termed multifractal detrending moving-average cross-correlation analysis (MFXDMA), which combines the ideas of MFDMA and DCCA. The main difference between MFXDFA and MFXDMA is that the latter adopts local moving average as the trend function. Since the MFDMA algorithm outperforms the MFDFA algorithm for multifractal time series, we expect that the MFXDMA algorithm will show advantages over the MFXDFA algorithm. Our numerical experiments and real-work data analysis confirm this conjecture.

The paper is organized as follows. Section II describes a unified framework of the MFXDFA and MFXDMA algorithms. Section III gives extensive numerical experiments using fractal and multifractal time series with known analytical expressions [bivariate fractional Brownian motions, two-component autoregressive fractionally integrated moving average (ARFIMA) processes, and binomial measures] to investigate the performance of the algorithms. In Sec. IV, we apply the algorithms to daily stock index returns and volatilities. We discuss and summarize our findings in Sec. V.

II. MFXDMA AND MFXDFA

Consider two stationary time series $\{x(i)\}$ and $\{y(i)\}$ of the same length M, where $i = 1,2,\ldots,M$. Without loss of generality, we can assume that these two time series have zero means. Each time series is covered with $M_s = [M/s]$ nonoverlapping boxes of size s. The profiles within the vth box $[l_v + 1, l_v + s]$, where $l_v = (v-1)s$, are determined to be

$$X_v(k) = \sum_{j=1}^{k} x(l_v + j), \quad Y_v(k) = \sum_{j=1}^{k} y(l_v + j), \quad (5)$$

where $k = 1,\ldots,s$. Assume that the local trending functions of $\{X_v(k)\}$ and $\{Y_v(k)\}$ are $\{\widetilde{X}_v(k)\}$ and $\{\widetilde{Y}_v(k)\}$, respectively. The cross correlation for each box is calculated as follows:

$$F_v(s) = \frac{1}{s} \sum_{k=1}^{s} [X_v(k) - \widetilde{X}_v(k)][Y_v(k) - \widetilde{Y}_v(k)]. \quad (6)$$

The qth order cross correlation is calculated as follows:

$$F_{xy}(q,s) = \left[\frac{1}{m} \sum_{v=1}^{m} |F_v(s)|^{q/2} \right]^{1/q} \quad (7)$$

when $q \neq 0$, and

$$F_{xy}(0,s) = \exp\left[\frac{1}{2m} \sum_{v=1}^{m} \ln |F_v(s)| \right]. \quad (8)$$

We then expect the following scaling relation:

$$F_{xy}(q,s) \sim s^{h_{xy}(q)}. \quad (9)$$

According to the standard multifractal formalism, the multifractal scaling exponent $\tau(q)$ can be used to characterize the multifractal nature, which reads

$$\tau_{xy}(q) = q h_{xy}(q) - D_f, \quad (10)$$

where D_f is the fractal dimension of the geometric support of the multifractal measure [9]. For time series analysis, we have $D_f = 1$. If the scaling exponent function $\tau(q)$ is a nonlinear function of q, the signal has a multifractal nature. It is easy to obtain the singularity strength function $\alpha(q)$ and the multifractal spectrum $f(\alpha)$ via the Legendre transform [62]

$$\begin{aligned} \alpha_{xy}(q) &= \mathrm{d}\tau_{xy}(q)/\mathrm{d}q \\ f_{xy}(q) &= q\alpha_{xy} - \tau_{xy}(q). \end{aligned} \quad (11)$$

There are many different methods for the determination of $\widetilde{X}_v$ and $\widetilde{Y}_v$. The local detrending functions could be polynomials [2,3], which recovers the MFDXA method [52]. The local detrending function could also be the moving averages [10,11], in which case the algorithm is called MFXDMA. To be more clear, we rename the MFDXA algorithm as MFXDFA, and all multifractal analysis algorithms

for cross correlations based on local detrending are termed multifractal detrending or detrended cross-correlation analysis (or MFDCCA). MFXDFA is an MFDCCA method based on DFA, and MFXDMA is an MFDCCA method based on DMA. When $X = Y$, MFXDFA in Ref. [52] reduces to MFDFA in Ref. [9], and MFXDMA reduces to MFDMA in Ref. [15]. We note that the extension of the MFDCCA algorithms to high dimensions is straightforward [52].

The moving-average function $\widetilde{Z}(t)$ of $Z \in \{X,Y\}$ in a moving window [13] can be calculated as follows:

$$\widetilde{Z}(t) = \frac{1}{n} \sum_{k=-\lfloor (n-1)\theta \rfloor}^{\lceil (n-1)(1-\theta) \rceil} Z(t-k), \tag{12}$$

where n is the window size, $\lfloor g \rfloor$ is the largest integer smaller than g, $\lceil g \rceil$ is the smallest integer larger than g, and θ is the position parameter with the value varying in the range $[0,1]$. Hence, the moving-average function considers $\lceil (n-1)(1-\theta) \rceil$ data points in the past and $\lfloor (n-1)\theta \rfloor$ points in the future. We consider three special cases in this paper. The first case, $\theta = 0$, refers to the backward moving average [18], in which the moving-average function $\widetilde{Z}(t)$ is calculated over all the past $n-1$ data points of the signal. The second case, $\theta = 0.5$, corresponds to the centered moving average [18], where $\widetilde{Z}(t)$ contains half past and half future information in each window. The third case, $\theta = 1$, is called the forward moving average, where $\widetilde{Z}(t)$ considers the trend of $n-1$ data points in the future. Usually, one chooses $n = s$ to obtain better results [15].

III. NUMERICAL EXPERIMENTS

In order to investigate the validity and performance of the proposed MFDCCA algorithms, we perform extensive numerical experiments using bivariate fractional Brownian motions (BFBMs) [34–36], two-component ARFIMA processes [40,63], and binomial measures generated from the multiplicative p model [64]. By definition, there is no multifractality in BFBMs and two-component ARFIMA processes. Therefore, the $h_{xy}(q)$ function is independent of q, and the $\tau_{xy}(q)$ function is linear. In contrast, binomial measures are expected to possess a multifractal nature. These three classes of time series are adopted to test the performance of the algorithms since the theoretical expressions of $H_{xx}(q)$ are known for individual time series and we know the theoretical expressions of $H_{xy}(q)$ for the first two classes and the numerical expression for the third class. Note that we have used H for theoretical values and h for estimated values below.

A. Bivariate fractional Brownian motions

A bivariate fractional Brownian motion $[x(t),y(t)]$ with parameters $\{H_{xx},H_{yy}\} \in (0,1)^2$ is a self-similar Gaussian process with stationary increments, where $x(t)$ and $y(t)$ are two univariate fractional Brownian motions with Hurst indices H_{xx} and H_{yy} and are the two components of the BFBM [34–36]. The basic properties of multivariate fractional Brownian motions have been extensively studied [34–36]. Particularly, it has been proven that the Hurst index H_{xy} of the cross correlation between the two components is [34–36,38]:

$$H_{xy} = (H_{xx} + H_{yy})/2. \tag{13}$$

This property allows us to investigate the performances of the proposed algorithms on a solid foundation.

An efficient simulation technique for univariate fractional Brownian motions (FBMs) relies upon the embedding of the covariance matrix into a circulant matrix, whose square root can be easily obtained by the discrete Fourier transform [65]. This method is an exact simulation algorithm provided that the circulant matrix is positive definite. This algorithm can be generalized to simulate bivariate FBMs, which embeds the circulant of a block Toeplitz covariance matrix and uses the fast Fourier transform to diagonalize the block circulant matrix [66]. A detailed description of the simulation procedure can be found in Refs. [35,36].

In the simulation algorithm, the two Hurst indexes H_{xx} and H_{yy} of the two univariate FBMs and their cross-correlation coefficient ρ are input arguments. We have generated a huge number of BFBMs, where H_{xx}, H_{yy}, and ρ all vary from 0.1 to 0.9 with a spacing of 0.1. For a given triple of (H_{xx},H_{yy},ρ), 100 repeated simulations are conducted, and 100 BFBMs with a length of 2^{16} are generated. In most cases, the positive-definiteness condition is not fulfilled. We then perform MFXDMA and MFXDFA on each BFBM to obtain the scaling exponent h_{xy}. The average over 100 repeated simulations is calculated. We have observed for each BFBM and each algorithm that

$$h_{xy} = (h_{xx} + h_{yy})/2. \tag{14}$$

Our main findings are the following: (1) The exponent h_{xy} is independent of the cross-correlation coefficient ρ. (2) The $h_{xy}(q)$ functions are independent of q, indicating that the BFBMs are monofractals. (3) All four algorithms give nice estimates h_{xy} of the scaling exponents, which are very close to the corresponding theoretical H_{xy} values. (4) The centered MFXDMA algorithm ($\theta = 0.5$) and the MFXDFA algorithms have comparative performance and perform better than the backward and forward MFXDMA algorithms ($\theta = 0$ and $\theta = 1$). Since there are too many results to present in a concise way, we present a part of the results to manifest these findings.

A typical example of the BFBM with $H_{xx} = 0.1$, $H_{yy} = 0.5$, and $\rho = 0.3$ is illustrated in Fig. 1(a), and the corresponding power-law dependence of the fluctuation functions $F_{xy}(q,s)$ with respect to the scale s for the four algorithms is shown in Fig. 1(b). For MFXDMA algorithms, s should not be too large due to the finite-size effect. The scaling ranges span over two orders of magnitude for the MFXDMA algorithms and three orders of magnitude for the MFXDFA algorithm. In the determination of the scaling exponents h_{xy}, we have used the same scaling ranges as in Fig. 1(b) for all the BFBMs, and nice power-law relationships are observed.

Figure 1(c) shows the $h_{xy}(q)$ functions for $H_{xx} = H_{yy} = 0.8$ and $\rho = 0.5$ (top panel) and for $H_{xx} = 0.1$, $H_{yy} = 0.5$, and $\rho = 0.3$ (bottom panel). Although there is a decreasing trend in each function, the theoretical functions $H_{xy}(q) = 0.8$ and $H_{xy}(q) = 0.3$ are well within the error bars, indicating that the $h_{xy}(q)$ functions are independent of the order q. Hence, the four algorithms are able to correctly capture the monofractal nature of the BFBMs. We focus on $q = 2$ below.

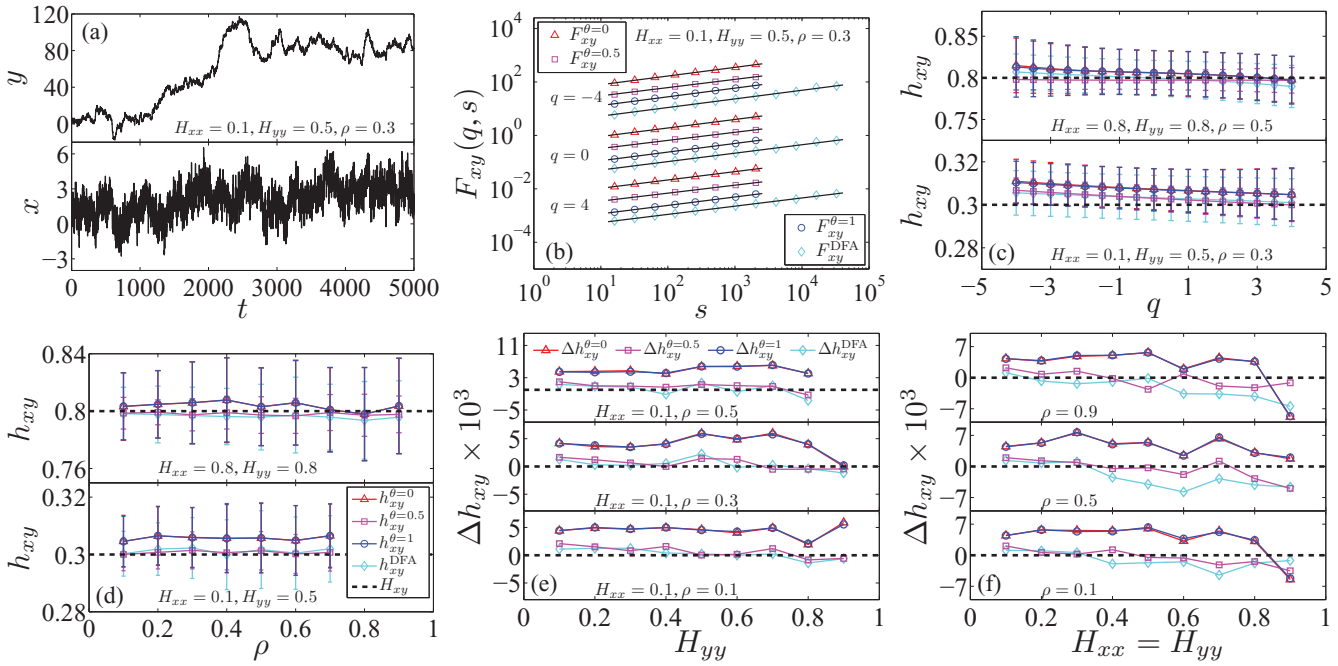

FIG. 1. (Color online) Multifractal detrended cross-correlation analysis of bivariate fractional Brownian motions. Comparisons are performed among three MFXDMA algorithms with $\theta = 0$, 0.5, and 1 and the MFXDFA algorithm. The results in (c)–(f) are averaged over 100 repeated simulations. (a) A typical example of BFBM with $H_{xx} = 0.1$, $H_{yy} = 0.5$, and $\rho = 0.3$. (b) Power-law dependence of the fluctuation functions $F_{xy}(q,s)$ of the BFBM shown in (a) with respect to the scale s for $q = -4$, $q = 0$, and $q = 4$. The straight lines are the best power-law fits to the data. The results have been translated vertically for better visibility. (c) Scaling exponents $h_{xy}(q)$ with the theoretical values as a dashed line for $H_{xx} = H_{yy} = 0.8$ and $\rho = 0.5$ (top) and $H_{xx} = 0.1$, $H_{yy} = 0.5$, and $\rho = 0.3$ (bottom). (d) Independence of the scaling exponents h_{xy} with respect to the cross-correlation coefficient ρ for $H_{xx} = H_{yy} = 0.8$ (top) and $H_{xx} = 0.1$ and $H_{yy} = 0.5$ (bottom). (e) Differences $\Delta h_{xy}(q)$ between the estimated scaling exponents h_{xy} and the theoretical exponents H_{xy} for BFBMs, where $H_{xx} = 0.1$ is fixed, H_{yy} varies from 0.1 to 0.9, and ρ takes different values. (f) Differences $\Delta h_{xy}(q)$ between h_{xy} and H_{xy} for BFBMs with $H_{xx} = H_{yy}$ varying from 0.1 to 0.9 and different ρ values.

Figure 1(d) shows the dependence of the scaling exponents h_{xy} with respect to the cross-correlation coefficient ρ for $H_{xx} = H_{yy} = 0.8$ (top panel) and for $H_{xx} = 0.1$ and $H_{yy} = 0.5$ (bottom panel). We find that the h_{xy} functions ($h_{xy}^{\theta=0}$, $h_{xy}^{\theta=0.5}$, $h_{xy}^{\theta=1}$ and h_{xy}^{DFA}) for the four algorithms are independent of ρ. This finding is very important since it distinguishes the temporal cross correlations quantified by MFDCCA algorithms and the cross-sectional correlation quantified by ρ. Two uncorrelated time series may exhibit long-term power-law cross correlation. In addition, the centered MFXDMA and the MFXDFA give similarly very accurate estimates of the scaling exponents with $h_{xy}^{\theta=0.5} \approx h_{xy}^{\mathrm{DFA}}$, $H_{xy} = 0.8$ for the top panel and $H_{xy} = 0.3$ for the bottom panel. In contrast, Fig. 1(d) shows that the backward and forward MFXDMA algorithms perform slightly worse and $h_{xy}^{\theta=0} \approx h_{xy}^{\theta=1}$.

In order to compare the performance of the four algorithms, we calculate the difference between the estimated exponent h_{xy} and the theoretical exponent H_{xy}:

$$\Delta h_{xy} = h_{xy} - H_{xy}. \tag{15}$$

Figure 1(e) shows the dependence of Δh_{xy} with respect to H_{yy} with a fixed $H_{xx} = 0.1$ for $\rho = 0.5$ (top panel), $\rho = 0.3$ (middle panel), and $\rho = 0.1$ (bottom panel), while Fig. 1(f) shows the dependence of Δh_{xy} with respect to $H_{xx} = H_{yy}$ for $\rho = 0.9$ (top panel), $\rho = 0.5$ (middle panel), and $\rho = 0.1$ (bottom panel). All the Δh_{xy} values in Figs. 1(e) and 1(f) are less than 0.01, implying that all the four algorithms give good estimates. It is interesting to observe that $h_{xy}^{\theta=0} \approx h_{xy}^{\theta=1}$ for all the cases. In addition, the centered MFXDMA and the MFXDFA algorithms outperform the backward and forward MFXDMA algorithms. We note that these conclusions also hold for other BFBMs. The relative performances between the centered MFXDMA and the MFXDFA algorithms are a little bit complicated. When $H_{xx} \neq H_{yy}$, as shown in Fig. 1(e), the two algorithms have comparable performance since $\Delta h_{xy}^{\theta=0.5} \approx \Delta h_{xy}^{\mathrm{DFA}} \approx 0$. When $H_{xx} = H_{yy}$, as shown in Fig. 1(f), the centered MFXDMA algorithm slightly outperforms the MFXDFA algorithm. In summary, the centered MFXDMA algorithm ($\theta = 0.5$) is recommended for analyzing bivariate fractional Brownian motions.

B. Two-component ARFIMA processes

The power-law autocorrelations in stochastic variables can be modeled by an ARFIMA process [67]:

$$z(t) = Z(d,t) + \epsilon(t), \tag{16}$$

where $d \in (0,0.5)$ is a memory parameter, ϵ_z is an independent and identically distributed Gaussian variable, and

$$Z(d,t) = \sum_{n=1}^{\infty} a_n(d) z(t-n), \tag{17}$$

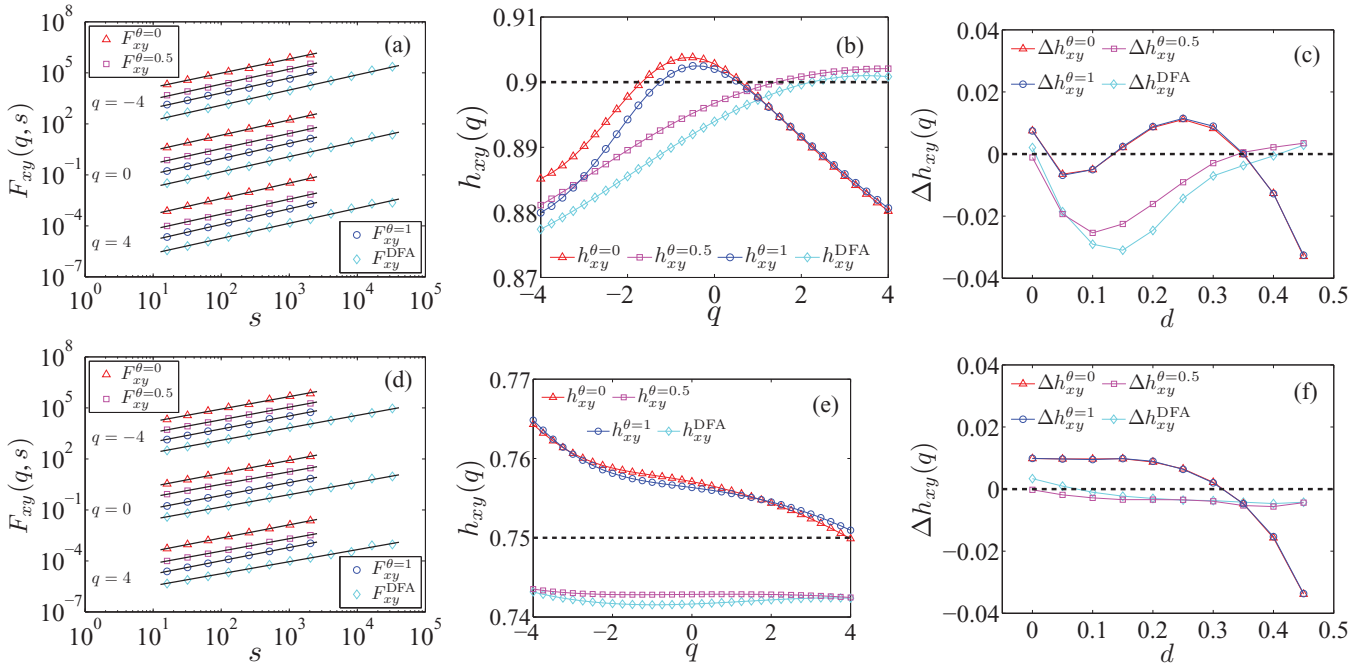

FIG. 2. (Color online) Multifractal detrended cross-correlation analysis of two-component ARFIMA processes. Comparisons are performed among three MFXDMA algorithms with $\theta = 0$, 0.5, and 1 and the MFXDFA method. (a) Power-law dependence of the fluctuation functions $F_{xy}(q,s)$ with respect to the scale s for $q = -4$, $q = 0$, and $q = 4$ for the process in Eq. (20) with $d_1 = d_2 = 0.4$. The straight lines are the best power-law fits to the data. The results have been translated vertically for better visibility. (b) Scaling exponents $h_{xy}(q)$ for the process in Eq. (20) with $d_1 = d_2 = 0.4$. (c) Differences Δh_{xy} between the estimated scaling exponents h_{xy} and the theoretical exponents H_{xy} for the process in Eq. (20) with different d values where $d_1 = d_2 = d$. (d) Power-law dependence of the fluctuation functions $F_{xy}(q,s)$ with respect to the scale s for $q = -4$, $q = 0$, and $q = 4$ for the process in Eq. (22) with $d_1 = 0.1$ and $d_2 = 0.4$. (e) Scaling exponents $h_{xy}(q)$ for the process in Eq. (22) with $d_1 = 0.1$ and $d_2 = 0.4$. (f) Differences Δh_{xy} between h_{xy} and H_{xy} for the process in Eq. (22) with different d values where $d_1 = d_2 = d$.

in which $a_n(d)$ is the weight,

$$a_n(d) = d\Gamma(n-d)/[\Gamma(1-d)\Gamma(n+1)]. \tag{18}$$

The Hurst index H_{zz} is related to the memory parameter d by [40,68]

$$H_{zz} = 0.5 + d. \tag{19}$$

For the two-component ARFIMA processes discussed below, we take $Z = X$ or Y.

The two-component ARFIMA process is defined as follows [63]:

$$\begin{aligned} x(t) &= WX(d_1,t) + (1-W)Y(d_2,t) + \epsilon_x(t) \\ y(t) &= (1-W)X(d_1,t) + WY(d_2,t) + \epsilon_y(t), \end{aligned} \tag{20}$$

where $W \in [0.5,1]$ quantifies the coupling strength between the two processes $x(t)$ and $y(t)$. When $W = 1$, $x(t)$ and $y(t)$ are fully decoupled and become two separate ARFIMA processes, as defined in Eq. (16). The cross correlation between $x(t)$ and $y(t)$ increases when W decreases from 1 to 0.5 [63]. To our knowledge, no general expression has been analytically derived for H_{xy}. When $d_1 > d_2$, the Hurst index H_{xx} of $x(t)$ decreases from $0.5 + d_1$ to certain value greater than $0.5 + d_2$ when W decreases from 1 to 0.5 [63]. In other words, H_{xx} locates within the interval $[0.5 + d_2, 0.5 + d_1]$. When $d_1 = d_2 = d$, i.e., $d_1 \to d_2$, we obtain

$$H_{xx} = H_{yy} = 0.5 + d, \tag{21}$$

which does not depend on the value of W.

When $W = 1$ and $\epsilon_x(t) = \epsilon_y(t) = \epsilon(t)$, the two-component ARFIMA process becomes [40]

$$\begin{aligned} x(t) &= X(d_1,t) + \epsilon(t) \\ y(t) &= Y(d_2,t) + \epsilon(t)\ . \end{aligned} \tag{22}$$

If x and y are long-range power-law cross-correlated, it has been analytically derived that Eq. (13) holds [44].

Figures 2(a)–2(c) show the results for the process in Eq. (20). Figure 2(a) illustrates in log-log scale the dependence of the fluctuation functions $F_{xy}(q,s)$ with respect to the scale s for $q = -4$, $q = 0$, and $q = 4$ for the process in Eq. (20) with $d_1 = d_2 = 0.4$. Nice power-law relations are observed, which are also evident for other (d_1,d_2) pairs. Figure 2(b) shows the corresponding scaling exponents $h_{xy}(q)$ for the process in Eq. (20) with $d_1 = d_2 = 0.4$. We note that the equation $h_{xy}(q) = [h_{xx}(q) + h_{yy}(q)]/2$ holds for all the four curves. For the four algorithms, $h_{xy}(q)$ is close to the horizontal line $H = 0.9$, indicating that all the four algorithms correctly unveil the fractal nature of the two-component ARFIMA process. For $q = 2$, Fig. 2(b) shows that the MFXDFA gives the best estimate of h_{xy}. Figure 2(c) depicts the differences Δh_{xy} between h_{xy} and H_{xy} with $q = 2$ for the process in Eq. (20) with different d values where $d_1 = d_2 = d$. It is found that (1) the two MFXDMA algorithms with $\theta = 0$ and $\theta = 1$ have the same performance, (2) the two MFXDMA algorithms with $\theta = 0$ and $\theta = 1$ perform better than the MFXDFA and the MFXDMA with $\theta = 0.5$ for relatively small d values,

and (3) the two MFXDMA algorithms with $\theta = 0$ and $\theta = 1$ perform worse for large d values.

Figures 2(d)–2(f) show the results for the process in Eq. (22). Figure 2(d) illustrates in log-log scale the dependence of the fluctuation functions $F_{xy}(q,s)$ with respect to the scale s for $q = -4$, $q = 0$, and $q = 4$ for the process in Eq. (22) with $d_1 = 0.1$ and $d_2 = 0.4$. Nice power-law relations are observed, which are also evident for other (d_1,d_2) pairs. Figure 2(e) shows the corresponding scaling exponents $h_{xy}(q)$ for the process in Eq. (22) with $d_1 = 0.1$ and $d_2 = 0.4$. Again, the equation $h_{xy}(q) = [h_{xx}(q) + h_{yy}(q)]/2$ holds for all the four curves. For the four algorithms, $h_{xy}(q)$ is close to the horizontal line $H = 0.75$, indicating that all the four algorithms correctly unveil the fractal nature of the two-component ARFIMA process. For $q = 2$, Fig. 2(e) shows that the MFXDMA algorithms with $\theta = 0$ and $\theta = 1$ give the best estimate of h_{xy}. Figure 2(f) shows the differences between h_{xy} and H_{xy} with $q = 2$ for the process in Eq. (22) with different d values where $d_1 = d_2 = d$. It is found that the MFXDFA and the MFXDMA with $\theta = 0.5$ outperform the other two algorithms and give comparably nice estimates.

He and Chen have investigated the two-component ARFIMA process defined in Eq. (20) of different lengths utilizing the DCCA method (the MFXDFA method with $q = 2$) and the DMCA method (the MFXDMA method with $\theta = 0$ and $q = 2$) and found that the DMCA method performs better in most cases and performs worse in a few cases [69]. However, both methods are prone to underestimate the exponents h_{xy} [69]. Our results shown in Fig. 2(c) are consistent with their results for $d = 0.15$, 0.25, and 0.35 in the sense that the MFXDMA method with $\theta = 0$ outperforms the MFXDFA method. However, we have obtained better estimates for h_{xy}, and there is no systematic underestimation. For instance, the three MFXDMA methods give $h_{xy} \approx 0.85$ or $\Delta h_{xy} \approx 0$ when $d = 0.35$, as shown in Fig. 2(c).

There are two subtle issues that might worsen the estimation of h_{xy}. Podobnik and Stanley [40] introduced a cutoff length $M = 10^4$ in their numerical simulations and let the sum run from 1 to M, i.e., they set $a_j = 0$ for $j > M$. Our numerical experiments show that this cutoff seems optimal and a smaller or larger cutoff will worsen the estimation of the exponents. This finding applies for both MFXDMA and MFXDFA. In addition, we stress that the upper bound of the scaling range for the MFXDMA algorithms should not be too large because each moving average is calculated within a window of size s. Let us take the MFXDMA algorithm with $\theta = 0$ as an example. In this case, the moving averages of the first $s - 1$ data points are not well defined. The bias becomes more significant for large window size s. When s is large, the $F_{xy}(q,s)$ function bends downward, and the overall slope flattens. Similar arguments apply for other MFXDMA algorithms with different θ values. In contrast, the MFXDFA algorithm does not suffer from this finite-size effect.

C. Multifractal binomial measures

We construct two binomial measures $\{x(i) : i = 1,2,\ldots,2^k\}$ and $\{y(i) : i = 1,2,\ldots,2^k\}$ from the p model with known analytic multifractal properties as the third example [64]. Each multifractal signal is obtained in an iterative way. We start with the zeroth iteration $k = 0$, where the data set $z(i)$ consists of one value, $z^{(0)}(1) = 1$. In the kth iteration, the data set $\{z^{(k)}(i) : i = 1,2,\ldots,2^k\}$ is obtained from

$$\begin{aligned} z^{(k)}(2i-1) &= p_z z^{(k-1)}(i) \\ z^{(k)}(2i) &= (1-p_z) z^{(k-1)}(i) \end{aligned} \tag{23}$$

for $i = 1,2,\ldots,2^{k-1}$. We notice that there are typos in the formula in Ref. [52]. When $k \to \infty$, $z^{(k)}(i)$ approaches a binomial measure, whose scaling exponent function $H_{zz}(q)$ has an analytic form [62,64],

$$H_{zz}(q) = 1/q - \log_2\left[p_z^q + (1-p_z)^q\right]/q. \tag{24}$$

According to Eq. (10), we have

$$\mathcal{T}_{zz}(q) = -\log_2\left[p_z^q + (1-p_z)^q\right]. \tag{25}$$

In our simulation, we have performed $k = 16$ iterations with $p_x = 0.3$ for $x(i)$ and $p_y = 0.4$ for $y(i)$. The analytic scaling exponent functions $H_{xx}(q)$ and $H_{yy}(q)$ of x and y are expressed in Eq. (24). The two time series x and y are strongly correlated with a coefficient of 0.82, which originates from the fact that the two sequences are constructed according to the same rules. The results are depicted in Fig. 3.

Figure 3(a) illustrates the power-law dependence of $F_{xy}(q,s)$ against s for the four algorithms. Since the time series is not very long, we investigate $-4 \leqslant q \leqslant 4$ to ensure the convergence of the qth moments [70,71]. For the MFXDMA algorithms, there is a finite-size effect since the moving averages at the ends of the time series are ill defined. This effect becomes significant, and the estimation of F_{xy} for large scales s deteriorates. The scaling range is chosen as $[2^4,2^{11}]$ for the three MFXDMA methods. In contrast, the MFXDFA method performs poorly if the same scaling range is adopted. We use $[2^8,2^{15}]$ for the MFXDFA method, which seems optimal. The algorithm-specific selection of the scaling range reveals the difference in the applicability of the two types of methods. Figure 3(a) shows that the power-law scaling is excellent for both positive and negative q values.

The power-law scaling exponents (h_{xy}^{DFA}, $h_{xy}^{\theta=0}$, $h_{xy}^{\theta=0.5}$, and $h_{xy}^{\theta=1}$) are presented in Fig. 3(b), while the mass scaling exponents (τ_{xy}^{DFA}, $\tau_{xy}^{\theta=0}$, $\tau_{xy}^{\theta=0.5}$, and $\tau_{xy}^{\theta=1}$) and the multifractal spectra (f_{xy}^{DFA}, $f_{xy}^{\theta=0}$, $f_{xy}^{\theta=0.5}$, and $f_{xy}^{\theta=1}$) are illustrated in Figs. 3(c) and 3(d), respectively. It is evident that the MFXDMA method with $\theta = 0.5$ fails in a large part to correctly estimate the exponents, while the other three methods work much better. This finding is consistent with the conclusion that the MFDMA method with $\theta = 0.5$ performs much worse than the MFDFA method and the MFDMA methods with $\theta = 0$ and $\theta = 1$ [15].

The insets of Fig. 3(b) show the interesting feature for all the four algorithms that

$$h_{xy}(q) = [h_{xx}(q) + h_{yy}(q)]/2 \tag{26}$$

no matter how accurate the estimates of an algorithm is. Similar relationships hold for individual monofractal ARFIMA signals [40] and individual binomial measures [15]. Hence, we can give the "theoretical" expression of $H_{xy}(q)$ as follows:

$$H_{xy}(q) = [H_{xx}(q) + H_{yy}(q)]/2, \tag{27}$$

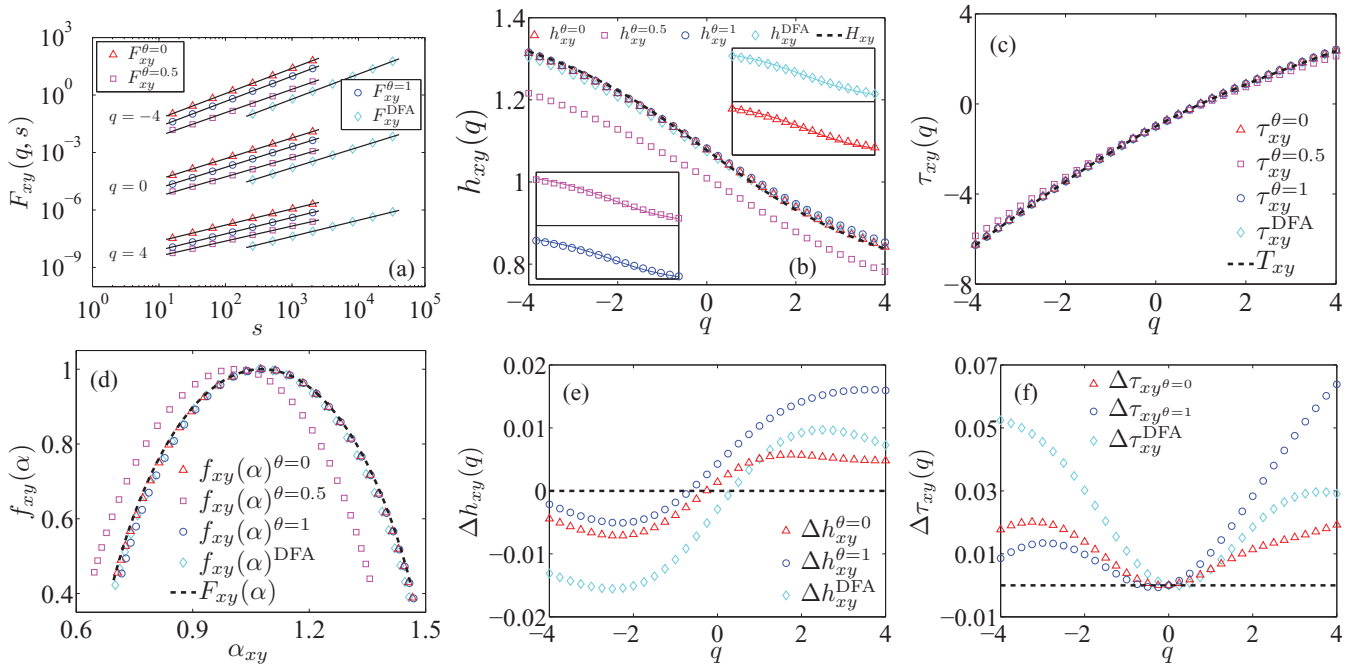

FIG. 3. (Color online) Multifractal detrended cross-correlation analysis of two cross-correlated binomial measures generated from the p model with $p_x = 0.3$ and $p_y = 0.4$. Comparisons are performed among three MFXDMA algorithms with $\theta = 0$, 0.5, and 1 and the MFXDFA method. (a) Power-law dependence of the fluctuation functions $F_{xy}(q,s)$ with respect to the scale s for $q = -4$, $q = 0$, and $q = 4$. The straight lines are the best power-law fits to the data. The results have been translated vertically for better visibility. (b) Scaling exponents $h_{xy}(q)$ with the theoretical values as a dashed line. The insets show the $h_{xy}(q)$ curves and the corresponding $[h_{xx}(q) + h_{yy}(q)]/2$ curves, verifying the relation $h_{xy}(q) = [h_{xx}(q) + h_{yy}(q)]/2$. (c) Multifractal mass exponents $\tau(q)$ obtained from the MFXDMA and MFXDFA methods, with the theoretical curve shown as a dashed line. (d) Multifractal spectra $f(\alpha)$ with respect to the singularity strength α for the four methods. The dashed curve is the theoretical multifractal spectrum. (e) Differences $\Delta h_{xy}(q)$ between the estimated mass exponents and their theoretical values for the three algorithms: MFXDFA, MFXDMA with $\theta = 0$, and MFXDMA with $\theta = 1$. (f) Differences $\Delta\tau(q)$ between the estimated mass exponents and their theoretical values for the three algorithms: MFXDFA, MFXDMA with $\theta = 0$, and MFXDMA with $\theta = 1$.

where $H_{xx}(q)$ and $H_{yy}(q)$ are given in Eq. (24). The theoretical line is plotted in Fig. 3(b) as a dashed line. According to Eq. (10), we obtain

$$\mathcal{T}_{xy}(q) = [\mathcal{T}_{xx}(q) + \mathcal{T}_{yy}(q)]/2, \tag{28}$$

which is shown in Fig. 3(c) for comparison. Similarly, we have

$$\mathcal{F}_{xy}(\alpha) = [\mathcal{F}_{xx}(\alpha) + \mathcal{F}_{yy}(\alpha)]/2, \tag{29}$$

which is illustrated in Fig. 3(d) as a dashed curve.

In order to further assess the performance of the MFXDFA method and the two MFXDMA methods with $\theta = 0$ and $\theta = 1$, we compare the empirical estimates of $h_{xy}(q)$ and $\tau_{xy}(q)$ with the theoretical values of $H_{xy}(q)$ and $\mathcal{T}_{xy}(q)$ by calculating the relative errors:

$$\Delta h_{xy}(q) = h_{xy}(q) - H_{xy}(q) \tag{30}$$

and

$$\Delta\tau_{xy}(q) = \tau_{xy}(q) - \mathcal{T}_{xy}(q), \tag{31}$$

which are shown in Figs. 3(e) and 3(f), respectively. Roughly speaking, the MFXDMA algorithm with $\theta = 1$ performs best and the MFXDFA algorithm performs worst for most negative q values, and the MFXDMA method with $\theta = 0$ performs best and the MFXDMA method with $\theta = 1$ performs worst for most negative q values. On average, the backward MFXDMA method ($\theta = 0$) has the best performance and is thus recommended.

IV. APPLICATION TO STOCK MARKET INDEX RETURNS AND VOLATILITIES

We now apply the MFXDMA algorithms to investigate the temporal cross correlations of the daily return and volatility time series of the Dow Jones Industrial Average (DJIA) and the National Association of Securities Dealers Automated Quotations (NASDAQ) index. The power-law cross correlations between the DJIA volatility and the NASDAQ volatility have been studied using the DCCA method [40] and the MFXDFA method [52]. The closing prices of the DJIA and the NASDAQ from 5 February 1971 to 25 January 2011 have been retrieved. The length of the time series is 10084 trading days. The return is defined as the daily difference of the logarithmic closing prices, and the volatility is defined as the absolute value of the return.

Figure 4(a) illustrates in log-log scale the dependence of the fluctuation functions $F_{xy}(q,s)$ with respect to the scale s for $q = -4$, $q = 0$, and $q = 4$ for the returns. Excellent power laws are observed spanning over two orders of magnitude for all the four algorithms. The resulting h_{xy} functions are shown in Fig. 4(b). All four h_{xy} functions are monotonically decreasing, indicating that the cross correlations between

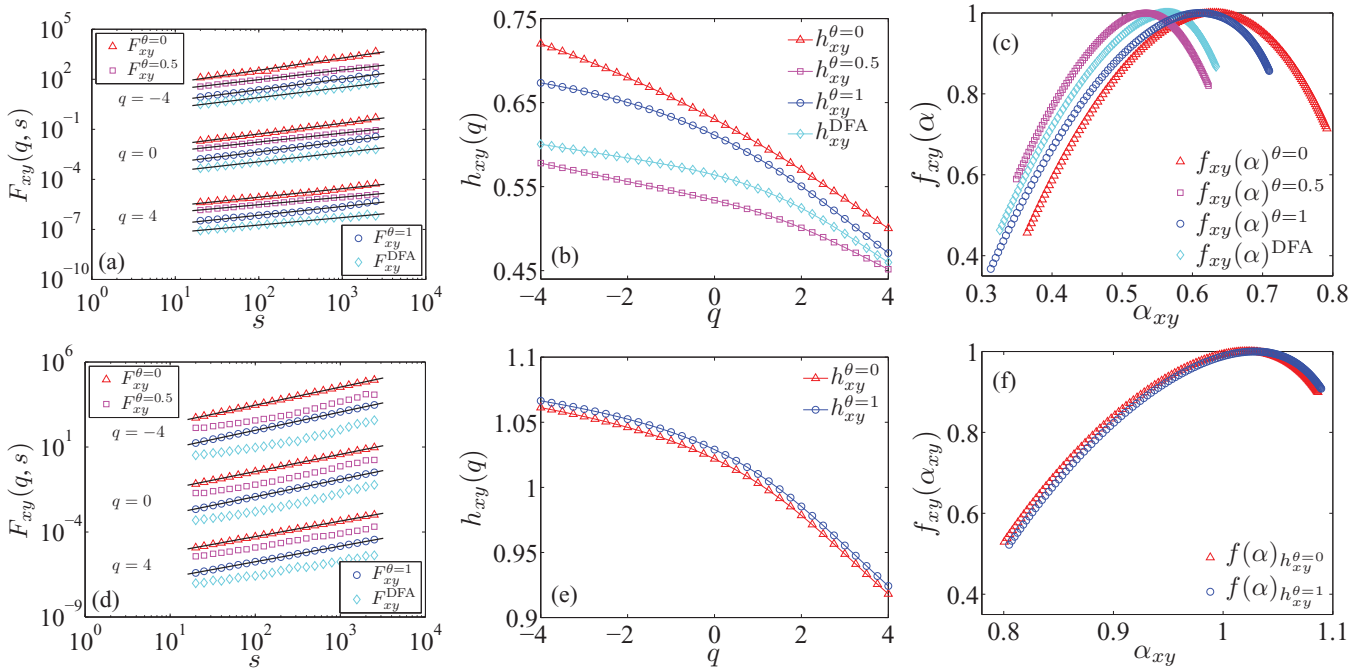

FIG. 4. (Color online) Multifractal detrended cross-correlation analysis of (a–c) the return time series and (d–f) the volatility time series for the DJIA index and the NASDAQ index. Comparisons are performed among three MFXDMA algorithms with $\theta = 0$, 0.5, and 1 and the MFXDFA method. (a, d) Dependence of the fluctuation functions $F_{xy}(q,s)$ with respect to the scale s for $q = -4$, $q = 0$, and $q = 4$. The straight lines are the best power-law fits to the data. The results have been translated vertically for better visibility. (b, e) Scaling exponents $h_{xy}(q)$ with respect to q. (c, f) Multifractal spectra $f_{xy}(\alpha)$ with respect to the singularity strength α.

the index returns exhibit a multifractal nature. We also find that

$$h_{xy}^{\theta=0}(q) > h_{xy}^{\theta=1}(q) > h_{xy}^{\mathrm{DFA}}(q) > h_{xy}^{\theta=0.5}(q) \qquad (32)$$

for $-4 \leqslant q \leqslant 4$. When $q = 2$, all the h_{xy} values are less than 0.6 and particularly $h_{xy}^{\theta=0.5} \approx 0.5$. This means that there is no significant linear long-term memory in the cross correlations of the returns. The multifractal spectra $f_{xy}(\alpha)$ are plotted in Fig. 4(c). The singularity widths are all significantly greater than 0, confirming that the cross correlations possess a multifractal nature.

Figure 4(d) illustrates in log-log scale the dependence of the fluctuation functions $F_{xy}(q,s)$ with respect to the scale s for $q = -4$, $q = 0$, and $q = 4$ for the volatilities. Excellent power-law scaling is observed in the fluctuation functions for the MFXDMA algorithms with $\theta = 0$ and 1. However, for the MFXDFA algorithm and the MFXDMA algorithm with $\theta = 0.5$, there is a crossover in each curve. If we treat each curve with two scaling ranges and perform analysis on each scaling range, the resulting $h_{xy}(q)$ functions are not monotonically decreasing, and the multifractal spectra $f_{xy}(\alpha)$ are not concave. We thus focus on the two MFXDMA algorithms with $\theta = 0$ and 1, which lead to one scaling range. The two $h_{xy}(q)$ functions are depicted in Fig. 4(e). The two functions are monotonically decreasing and close to each other. When $q = 2$, h_{xy} is close to 0.98, showing a very strong linear long-term memory in the cross correlations between volatilities. We note that the relation $h_{xy}(q) = [h_{xx}(q) + h_{yy}(q)]/2$ does not hold, which is consistent with previous work [52]. Figure 4(f) plots the two multifractal spectra. The large singularity width means that the cross correlations between the two index volatilities exhibit a multifractal nature.

Our results for the volatility seem different from those in Refs. [40,52]. First of all, the DJIA and NASDAQ time series are much longer in the current work. More importantly, the power-law scaling in the previous works exhibits significant fluctuations [40,52], which makes it difficult to determine a proper scaling range. According to Fig. 4(d), it is evident that the MFXDMA algorithms with $\theta = 0$ and 1 significantly outperform the MFXDFA algorithm.

V. CONCLUSION AND DISCUSSION

In this work, we have developed a class of MFDCCA algorithms based on the detrending moving-average analysis. The performances of the MFXDMA algorithms are compared with the MFXDFA method by extensive numerical experiments on pairs of time series generated from bivariate fractional Brownian motions, two-component autoregressive fractionally integrated moving-average processes, and binomial measures, which have theoretical expressions of the multifractal nature. In all cases, the scaling exponents h_{xy} extracted from the MFXDMA and MFXDFA algorithms are very close to the theoretical values.

For bivariate fractional Brownian motions, the scaling exponent h_{xy} of the cross correlation is found to be independent of the cross-correlation coefficient ρ between two time series. The MFXDFA and centered MFXDMA algorithms outperform the forward and backward MFXDMA algorithms. When $H_{xx} \neq H_{yy}$, the MFXDFA and centered MFXDMA

algorithms show comparable performance. When $H_{xx} = H_{yy}$, the centered MFXDMA algorithm performs slightly better than the MFXDFA algorithm. Our numerical experiments verified the validity of the BFBM generating algorithm [35,36,66]. For two-component autoregressive fractionally integrated moving-average processes, we also found that the MFXDFA and centered MFXDMA algorithms have comparative performances, while the forward and backward MFXDMA algorithms perform slightly worse. All four algorithms are able to correctly unveil the monofractal nature in the cross correlations between the components of BFBMs and two-component ARFIMA processes. For binomial measures, the forward MFXDMA algorithm exhibits the best performance, the centered MFXDMA algorithms performs worst, and the backward MFXDMA algorithm outperforms the MFXDFA algorithm when the moment order $q < 0$ and underperforms when $q > 0$.

In all three mathematical models, the relation $h_{xy} = (h_{xx} + h_{yy})/2$ has been confirmed for all four algorithms, where h_{xy}, h_{xx}, and h_{yy} are estimated scaling exponents. Previous works have shown that the MFDFA and MFDMA algorithms are able to give nice estimates for univariate signals, that is, $h_{xx} \approx H_{xx}$ and $h_{yy} \approx H_{yy}$. It follows immediately that $h_{xy} \approx (H_{xx} + H_{yy})/2$. Combining the theoretical fact that $H_{xy} \approx (H_{xx} + H_{yy})/2$, we obtain $H_{xy} \approx h_{xy}$. For monofractal time series, extensive numerical experiments unveiled that the performance of the DMA algorithms is comparable to the DFA algorithm and the centered DMA algorithm performs slightly better than DFA under certain situations [17–19]. This explains our numerical results for BFBMs and two-component ARFIMA processes. For multifractal measures generated from the p model, the backward MFDMA algorithm performs best [15], which explains our findings for MFDCCA algorithms.

We applied these algorithms to the returns and volatilities of two US stock market indexes. For the returns, the centered MFXDMA algorithm gives the best estimates of $h_{xy}(q)$ since its $h_{xy}(2)$ is closest to 0.5, and the MFXDFA algorithm has the second best performance. For the volatilities, the forward and backward MFXDMA algorithms give similar results, while the centered MFXDMA and the MFXDFA algorithms fail to extract a rational multifractal nature. These two applications are interesting since they showed that the choice of algorithms is automatic, although we did not know which one should be used before the analysis. The key message of our work is that we should use all four algorithms and compare the results to make a choice.

We note that the MFXDMA algorithms are easy to implement (see the Supplemental Material [72]).

ACKNOWLEDGMENTS

We are grateful to Jean-François Coeurjolly for providing the R code to generate bivariate fractional Brownian motions and to Anna Carbone, Gao-Feng Gu, Boris Podobnik, and Qun-Zhi Zhang for invaluable discussions. This work was partially supported by the National Natural Science Foundation of China under Grant No. 11075054 and the Fundamental Research Funds for the Central Universities.

APEENDIX: HIGHER-DIMENSIONAL MFXDMA

In this work, we have focused on time series analysis. It is easy to generalize the one-dimensional MFXDMA algorithms to higher dimensions. The higher-dimensional MFXDMA algorithms are closely related to the MFXDFA algorithms [52], the DMA algorithms [21], and the MFDMA algorithms [15] in higher dimensions.

Consider two physical quantities in d dimensions: $\{X(i_1, \ldots, i_d)\}$ and $\{Y(i_1, \ldots, i_d)\}$, where $i_j = 1,2, \ldots, N_j$ for $j = 1,2, \ldots, d$. Before proceeding, we need to construct the difference matrices $\{x(i_1, \ldots, i_d)\}$ and $\{y(i_1, \ldots, i_d)\}$ of X and Y. For simplicity, we denote $Z \in \{X,Y\}$ and z as the corresponding difference matrix, which are related by the following equation:

$$Z(i_1, \ldots, i_d) = \sum_{j_1=1}^{i_1} \cdots \sum_{j_d=1}^{i_d} z(i_1, \ldots, i_d). \tag{A1}$$

The matrix z is expressed as a square block matrix of size 2^d, whose block is $z(i_1, \ldots, i_d)$, where the intervals $I_j = i_j$ or $[1 : i_j - 1]$ for $j = 1,2, \ldots, d$. In real-world applications, we can focus on $d = 2$ and $d = 3$.

For the two-dimensional case $d = 2$, the four blocks are $z(i_1,i_2)$, $z(i_1 - 1,i_2)$, $z(i_1,1 : i_2 - 1)$, and $z(1 : i_1 - 1,1 : i_2 - 1)$. According to Eq. (A1), we have

$$Z(i_1,i_2) = z(i_1,i_2) + \sum_{j=1}^{i_1-1} z(j,i_2) + \sum_{j=1}^{i_2-1} z(i_2,j) + \sum_{j_1=1}^{i_1-1} \sum_{j_2=1}^{i_2-1} z(j_1,j_2). \tag{A2}$$

Since

$$\sum_{j_1=1}^{i_1-1} \sum_{j_2=1}^{i_2-1} z(j_1,j_2) = Z(i_1 - 1,i_2 - 1),$$

$$\sum_{j=1}^{i_1-1} z(j,i_2) = Z(i_1 - 1,i_2) - Z(i_1 - 1,i_2 - 1),$$

$$\sum_{j=1}^{i_2-1} z(i_2,j) = Z(i_1,i_2 - 1) - Z(i_1 - 1,i_2 - 1),$$

it follows that

$$z(i_1,i_2) = Z(i_1,i_2) + Z(i_1 - 1,i_2 - 1) - Z(i_1 - 1,i_2) - Z(i_1,i_2 - 1), \tag{A3}$$

where $Z(i,j) \triangleq 0$ if $i \times j = 0$.

For the three-dimensional case $d = 3$, the eight blocks are $z(i_1,i_2,i_3)$, $z(1 : i_1 - 1,i_2,i_3)$, $z(i_1,1 : i_2 - 1,i_3)$, $z(i_1,i_2,1 : i_3 - 1)$, $z(1 : i_1 - 1,1 : i_2 - 1,i_3)$, $z(1 : i_1 - 1,i_2,1 : i_3 - 1)$, $z(i_1,1 : i_2 - 1,1 : i_3 - 1)$, and $z(1 : i_1 - 1,1 : i_2 - 1,1 : i_3 - 1)$. We can derive similar to the two-dimensional case that

$$\begin{aligned} z(i_1,i_2,i_3) = {} & Z(i_1,i_2,i_3) - Z(i_1 - 1,i_2 - 1,i_3 - 1) \\ & + Z(i_1 - 1,i_2 - 1,i_3) + Z(i_1 - 1,i_2,i_3 - 1) \\ & + Z(i_1,i_2 - 1,i_3 - 1) - Z(i_1 - 1,i_2,i_3) \\ & - Z(i_1,i_2 - 1,i_3) - Z(i_1,i_2,i_3 - 1), \end{aligned} \tag{A4}$$

where $Z(i,j,k) \triangleq 0$ if $i \times j \times k = 0$. When $i_3 = 1$, Eq. (A4) reduces to Eq. (A3).

The algorithm of d-dimensional multifractal detrending moving-average cross-correlation analysis is described as follows.

Step 1. For each quantity $z = x$ or $z = y$, determine the moving averages $\widetilde{Z}(i_1,\ldots,i_d)$, where $s_j \leqslant i_j \leqslant N_j - \lfloor (s_j-1)\theta_1 \rfloor$ and $\{\theta_j\}$ are the position parameters with the values varying in the range $[0,1]$ for $j = 1,2,\ldots,d$. For each point located at $(i_1,\ldots,i_d)$ in the d-dimensional space, we extract a submatrix $z(k_1,\ldots,k_d)$ with size $s_1 \times \cdots \times s_d$ from the matrix z, where $k_j \in [i_j - \lceil (s_j-1)(1-\theta_j) \rceil, i_j + \lfloor (s_j-1)\theta_j \rfloor] \triangleq [m_{j,1}, m_{j,2}]$. We calculate the cumulative sums $Z'(k_1,\ldots,k_d)$ of the points within the box:

$$Z'(k_1,\ldots,k_d) = \sum_{\ell_1=m_{1,1}}^{k_1} \cdots \sum_{\ell_1=m_{d,1}}^{k_2} z(\ell_1,\ldots,\ell_d), \quad \text{(A5)}$$

and the moving average $\widetilde{Z}(i_1,\ldots,i_d)$ at location $(i_1,\ldots,i_d)$ is calculated as follows:

$$\widetilde{Z} = \frac{1}{s_1 \cdots s_d} \sum_{k_1=m_{1,1}}^{m_{1,2}} \cdots \sum_{k_1=m_{d,1}}^{m_{d,2}} Z'(k_1,\ldots,k_d). \quad \text{(A6)}$$

Step 2. For each quantity, calculate the cumulative sums $Q(i_1,\ldots,i_d)$ in a sliding window with size $s_1 \times \cdots \times s_d$, where $s_j \leqslant i_j \leqslant N_j - \lfloor (s_j-1)\theta_j \rfloor$. For each point located at $(i_1,\ldots,i_d)$, we have

$$Q = \sum_{k_1=i_1-s_1+1}^{i_1} \cdots \sum_{k_d=i_d-s_d+1}^{i_d} z(k_1,\ldots,k_d). \quad \text{(A7)}$$

Step 3. Detrend the matrix by removing the moving-average function $\widetilde{Z}(i_1,\ldots,i_d)$ from $Q(i_1,\ldots,i_d)$, and obtain the residual matrix $\epsilon_z(i_1,i_2)$ as follows:

$$\epsilon^z(i_1,\ldots,i_d) = Q(i_1,\ldots,i_d) - \widetilde{Z}(i_1,\ldots,i_d), \quad \text{(A8)}$$

where $s_j \leqslant i_j \leqslant N_j - \lfloor (s_j-1)\theta_j \rfloor$.

Step 4. Each residual matrix $\epsilon_z(i_1,\ldots,i_d)$ is partitioned into $N_{s_1} \times \cdots \times N_{s_d}$ disjoint boxes of the same size $s_1 \times \cdots \times s_d$, where $N_{s_j} = \lfloor [N_j - s_j(1+\theta_j)]/s_j \rfloor$. Each box can be denoted by $\epsilon^z_{v_1,\ldots,v_d}$ for $v_j = 1,\ldots,N_{s_j}$ such that $\epsilon^z_{v_1,\ldots,v_d}(k_1,\ldots,k_d) = \epsilon^z(l_{v_1}+k_1,\ldots,l_{v_d}+k_d)$ for $1 \leqslant k_j \leqslant s_j$, where $l_{v_j} = v_j s_j$. The cross correlation between X and Y in each box is calculated as follows:

$$F_{v_1,\ldots,v_d} = \frac{1}{s_1 \cdots s_d} \sum_{k_1=1}^{s_1} \cdots \sum_{k_d=1}^{s_d} \epsilon^x_{v_1,\ldots,v_d}(k_1,\ldots,k_d) \times \epsilon^y_{v_1,\ldots,v_d}(k_1,\ldots,k_d). \quad \text{(A9)}$$

Step 5. The qth order overall detrending cross-correlation function $F_q(n)$ is calculated as follows:

$$[F_q(s)]^q = \frac{1}{N_{s_1} \cdots N_{s_d}} \sum_{v_1=1}^{N_{s_1}} \cdots \sum_{v_d=1}^{N_{s_d}} |F_{v_1,\ldots,v_d}|^{q/2}, \quad \text{(A10)}$$

where $s^2 = \sum_{j=1}^d s_j^2/d$ and q can take any real values except for $q = 0$. When $q = 0$, we have

$$\ln[F_0(s)] = \frac{1}{N_{s_1} \cdots N_{s_d}} \sum_{v_1=1}^{N_{s_1}} \cdots \sum_{v_d=1}^{N_{s_d}} \ln |F_{v_1,\ldots,v_d}|, \quad \text{(A11)}$$

according to L'Hôpital's rule.

Step 6. Varying the box sizes s_j, we are able to determine the power-law relation between the fluctuation function $F_q(s)$ and the scale s,

$$F_q(s) \sim s^{h(q)}. \quad \text{(A12)}$$

In real-world applications, one usually uses $s_1 = \cdots = s_d = s$. When $N_{s_j} \neq [N_j - s_j(1+\theta_j)]/s_j$, one needs to start from different directions as for the DFA algorithm [73] or uses a random algorithm [74]. In addition, the box-by-box procedure is crucial for multifractal analysis, which was shown for high-dimensional MFDFA [20] and MFDMA [15]. However, the "traditional" procedure works well for high-dimensional fractals [21].

[1] B. B. Mandelbrot, *The Fractal Geometry of Nature* (Freeman, New York, 1983).

[2] C.-K. Peng, S. V. Buldyrev, S. Havlin, M. Simons, H. E. Stanley, and A. L. Goldberger, Phys. Rev. E **49**, 1685 (1994).

[3] K. Hu, P. C. Ivanov, Z. Chen, P. Carpena, and H. E. Stanley, Phys. Rev. E **64**, 011114 (2001).

[4] Z. Chen, P. C. Ivanov, K. Hu, and H. E. Stanley, Phys. Rev. E **65**, 041107 (2002).

[5] Z. Chen, K. Hu, P. Carpena, P. Bernaola Galvan, H. E. Stanley, and P. C. Ivanov, Phys. Rev. E **71**, 011104 (2005).

[6] Q. D. Y. Ma, R. P. Bartsch, P. Bernaola Galván, M. Yoneyama, and P. C. Ivanov, Phys. Rev. E **81**, 031101 (2010).

[7] A. Castro e Silva and J. G. Moreira, Phys. A **235**, 327 (1997).

[8] R. O. Weber and P. Talkner, J. Geophys. Res. **106**, 20131 (2001).

[9] J. W. Kantelhardt, S. A. Zschiegner, E. Koscielny-Bunde, S. Havlin, A. Bunde, and H. E. Stanley, Phys. A **316**, 87 (2002).

[10] N. Vandewalle and M. Ausloos, Phys. Rev. E **58**, 6832 (1998).

[11] E. Alessio, A. Carbone, G. Castelli, and V. Frappietro, Eur. Phys. J. B **27**, 197 (2002).

[12] J. Alvarez-Ramirez, E. Rodriguez, and J. C. Echeverría, Phys. A **354**, 199 (2005).

[13] S. Arianos and A. Carbone, Phys. A **382**, 9 (2007).

[14] A. Carbone, in *Science and Technology for Humanity (TIC-STH), 2009 IEEE Toronto International Conference* (IEEE, Piscataway, NJ, 2009), p. 691.

[15] G.-F. Gu and W.-X. Zhou, Phys. Rev. E **82**, 011136 (2010).

[16] A. Y. Schumann and J. W. Kantelhardt, Phys. A **390**, 2637 (2011).

[17] D. Grech and Z. Mazur, Acta Phys. Pol. B **36**, 2403 (2005).

[18] L. M. Xu, P. C. Ivanov, K. Hu, Z. Chen, A. Carbone, and H. E. Stanley, Phys. Rev. E **71**, 051101 (2005).

[19] A. Bashan, R. Bartsch, J. W. Kantelhardt, and S. Havlin, Phys. A **387**, 5080 (2008).
[20] G.-F. Gu and W.-X. Zhou, Phys. Rev. E **74**, 061104 (2006).
[21] A. Carbone, Phys. Rev. E **76**, 056703 (2007).
[22] C. Türk, A. Carbone, and B. M. Chiaia, Phys. Rev. E **81**, 026706 (2010).
[23] R. A. Antonia and C. W. Van Atta, J. Fluid Mech. **67**, 273 (1975).
[24] C. Meneveau, K. R. Sreenivasan, P. Kailasnath, and M. S. Fan, Phys. Rev. A **41**, 894 (1990).
[25] F. Schmitt, D. Schertzer, S. Lovejoy, and Y. Brunet, Europhys. Lett. **34**, 195 (1996).
[26] G. Xu, R. A. Antonia, and S. Rajagopalan, Europhys. Lett. **49**, 452 (2000).
[27] G. Xu, R. A. Antonia, and S. Rajagopalan, Europhys. Lett. **79**, 44001 (2007).
[28] A. N. Kravchenko, D. G. Bullock, and C. W. Boast, Agron. J. **92**, 1279 (2000).
[29] T. B. Zeleke and B.-C. Si, Agron. J. **96**, 1082 (2004).
[30] D.-C. Lin, Phys. A **387**, 3461 (2008).
[31] F. J. Jiménez-Hornero, J. E. Jiménez-Hornero, E. G. de Ravé, and P. Pavon-Domínguez, Environ. Monit. Assess. **167**, 675 (2010).
[32] D.-C. Lin and A. Sharif, Chaos **20**, 023121 (2010).
[33] F. J. Jiménez-Hornero, P. Pavón-Domínguez, E. G. de Rave, and A. B. Ariza-Villaverde, Atoms. Res. **99**, 366 (2011).
[34] F. Lavancier, A. Philippe, and D. Surgailis, Stat. Prob. Lett. **79**, 2415 (2009).
[35] J.-F. Coeurjolly, P.-O. Amblard, and S. Achard, Eur. Signal Process. Conf. **18**, 1567 (2010).
[36] P.-O. Amblard, J.-F. Coeurjolly, F. Lavancier, and A. Philippe, Bull. Soc. Math. Fr. (to be published).
[37] B. Podobnik, D. Wang, D. Horvatic, I. Grosse, and H. E. Stanley, Europhys. Lett. **90**, 68001 (2010).
[38] S. Arianos and A. Carbone, J. Stat. Mech. P03037 (2009).
[39] W. C. Jun, G. Oh, and S. Kim, Phys. Rev. E **73**, 066128 (2006).
[40] B. Podobnik and H. E. Stanley, Phys. Rev. Lett. **100**, 084102 (2008).
[41] D. Horvatic, H. E. Stanley, and B. Podobnik, Europhys. Lett. **74**, 18007 (2011).
[42] T. Qiu, B. Zheng, and G. Chen, New J. Phys. **12**, 043057 (2010).
[43] T. Qiu, G. Chen, L.-X. Zhong, and X.-W. Lei, Phys. A **390**, 828 (2011).
[44] B. Podobnik, I. Grosse, D. Horvatic, S. Ilic, P. Ch. Ivanov, and H. E. Stanley, Eur. Phys. J. B **71**, 243 (2009).
[45] G. F. Zebende, Phys. A **390**, 614 (2011).
[46] B. Podobnik, D. Horvatic, A. M. Petersen, and H. E. Stanley, Proc. Natl. Acad. Sci. USA **106**, 22079 (2009).
[47] E. L. Siqueira Jr., T. Stošić, L. Bejan, and B. Stošić, Phys. A **389**, 2739 (2010).
[48] N. Xu, P.-J. Shang, and S. Kamae, Nonlinear Dyn. **61**, 207 (2010).
[49] G. F. Zebende, P. A. da Silva, and A. M. Filho, Phys. A **390**, 1677 (2011).
[50] S. Achard, D. S. Bassett, A. Meyer-Lindenberg, and E. Bullmore, Phys. Rev. E **77**, 036104 (2008).
[51] H. Wendt, A. Scherrer, P. Abry, and S. Achard, in *2009 IEEE International Conference on Acoustics, Speech and Signal Processing* (IEEE, Piscataway, NJ, 2009), pp. 2913–2916.
[52] W.-X. Zhou, Phys. Rev. E **77**, 066211 (2008).
[53] L. Kristoufek, UTIA AV CR Research Report No. 2281, 2010 (unpublished).
[54] S. Shadkhoo and G. R. Jafari, Eur. Phys. J. B **72**, 679 (2009).
[55] S. Hajian and M. S. Movahed, Phys. A **389**, 4942 (2010).
[56] Y.-D. Wang, Y. Wei, and C.-F. Wu, Phys. A **389**, 5468 (2010).
[57] J.-L. Sun and H.-Y. Sheng, in *Third International Conference on Business Intelligence and Financial Engineering (BIFE)*, edited by L.-A. Yu, K.-K. Lai, and S.-Y. Wang (IEEE Computer Society, Tokyo, 2010), pp. 301–304.
[58] L.-Y. He and S.-P. Chen, Phys. A **390**, 297 (2011).
[59] L.-Y. He and S.-P. Chen, Chaos Solitons Fractals **44**, 355 (2011).
[60] Y.-D. Wang, Y. Wei, and C.-F. Wu, Phys. A **390**, 864 (2011).
[61] X.-J. Zhao, P.-J. Shang, A.-J. Lin, and G. Chen, Phys. A (to be published).
[62] T. C. Halsey, M. H. Jensen, L. P. Kadanoff, I. Procaccia, and B. I. Shraiman, Phys. Rev. A **33**, 1141 (1986).
[63] B. Podobnik, D. Horvatic, A.-L. Ng, H. E. Stanley, and P. C. Ivanov, Phys. A **387**, 3954 (2008).
[64] C. Meneveau and K. R. Sreenivasan, Phys. Rev. Lett. **59**, 1424 (1987).
[65] A. T. A. Wood and G. Chan, J. Comput. Graph. Stat. **3**, 409 (1994).
[66] G. Chan and A. T. A. Wood, Stat. Comput. **9**, 265 (1999).
[67] J. R. M. Hosking, Biometrika **68**, 165 (1981).
[68] B. Podobnik, P. Ch. Ivanov, K. Biljakovic, D. Horvatic, H. E. Stanley, and I. Grosse, Phys. Rev. E **72**, 026121 (2005).
[69] L.-Y. He and S.-P. Chen, Phys. A (to be publihsed).
[70] V. S. L'vov, E. Podivilov, A. Pomyalov, I. Procaccia, and D. Vandembroucq, Phys. Rev. E **58**, 1811 (1998).
[71] W.-X. Zhou, D. Sornette, and W.-K. Yuan, Phys. D **214**, 55 (2006).
[72] See Supplemental Material at http://link.aps.org/supplemental/10.1103/PhysRevE.84.016106 for the MATLAB codes implementing the 1D MFXDMA algorithms.
[73] J. W. Kantelhardt, E. Koscielny-Bunde, H. H. A. Rego, S. Havlin, and A. Bunde, Phys. A **295**, 441 (2001).
[74] L.-J. Ji, W.-X. Zhou, H.-F. Liu, X. Gong, F.-C. Wang, and Z.-H. Yu, Phys. A **388**, 3345 (2009).